1 Mixing state of oxalic acid containing particles in the rural area of Pearl

2 River Delta, China: implications for the formation mechanism of oxalic

3 acid

5 Chunlei Cheng[1,2], Mei Li[1,2*], Chak K. Chan[3], Haijie Tong[4], Changhong Chen[5],
6 Duohong Chen[6], Dui Wu[1,2], Lei Li[1,2], Cheng Wu[1,2], Peng Cheng[1,2], Wei Gao[1,2],
7 Zhengxu Huang[1,2], Xue Li[1,2], Zhijuan Zhang[1,2], Zhong Fu[7], Yanru Bi[7], Zhen Zhou[1,2*]
8
9
10 [1]Institute of Mass Spectrometer and Atmospheric Environment, Jinan University,
11 Guangzhou 510632, China
12 [2]Guangdong Provincial Engineering Research Center for on-line source apportionmen
13 t system of air pollution, Guangzhou 510632, China
14 [3]School of Energy and Environment, City University of Hong Kong, Hong Kong,
15 China
16 [4]Max Planck Institute for Chemistry, Multiphase Chemistry Department,
17 Hahn-Meitner-Weg 1, 55128 Mainz, Germany
18 [5]State of Environmental Protection Key Laboratory of the formation and prevention of
19 urban air pollution complex, Shanghai Academy of Environmental Sciences, Shanghai
20 200233, China
21 [6] State Environmental Protection Key Laboratory of Regional Air Quality Monitoring,
22 Guangdong Environmental Monitoring Center, Guangzhou, 510308, China
23 [7]Guangzhou Hexin Analytical Instrument Limited Company, Guangzhou 510530,
24 China
25
26
27 *Correspondence to*: Mei Li (limei2007@163.com) and Zhen Zhou (zhouzhen@gig.ac.cn)
28 Tel: 86-20-85225991, Fax: 86-20-85225991

30
31
32
33
34
35
36
37
38
39
40
41

Abstract:

The formation of oxalic acid and its mixing state in atmospheric particulate matter (PM) were studied using a single particle aerosol mass spectrometer (SPAMS) in the summer and winter of 2014 in Heshan, a supersite in the rural area of the Pearl River Delta (PRD) region in China. Oxalic acid-containing particles accounted for 2.5% and 2.7% in total detected ambient particles in summer and winter, respectively. Oxalic acid was measured in particles classified as elemental carbon (EC), organic carbon (OC), elemental and organic carbon (ECOC), biomass burning (BB), heavy metal (HM), secondary (Sec), sodium-potassium (NaK) and dust. Oxalic acid was found predominantly mixing with sulfate and nitrate during the whole sampling period, likely due to aqueous phase reactions. In summer, oxalic acid-containing particle number and ozone concentration followed a very similar trend, which may reflect the significant contribution of photochemical reactions to oxalic acid formation. The HM type particles were the most abundant oxalic acid particles in summer and the diurnal variations of peak area of iron and oxalic acid show opposite trends, which suggest a possible loss of oxalic acid through the photolysis of iron oxalato complexes during the strong photochemical activity period. In wintertime, carbonaceous type particles contained a substantial amount of oxalic acid as well as abundant carbon clusters and biomass burning markers. The general existence of nitric acid in oxalic acid-containing particles indicates an acidic environment during the formation process of oxalic acid. The peak areas of nitrate, sulfate and oxalic had similar temporal change in the carbonaceous type oxalic acid particles, and the organosulfate-containing oxalic acid particles well correlated with total oxalic acid particles during the episode, which suggests the formation of oxalic acid is closely associated with the oxidation of organic precursors in aqueous phase.

Keywords: Oxalic acid; Single particles; Mixing state; Photochemical process; Aqueous phase reactions.

1. Introduction

Organic aerosol, typically a large fraction of fine particles, contains more than thousands of organic compounds and contributes to visibility reduction, photochemical smog, climate change and adverse health effects (Novakov and Penner, 1993;Goldstein and Galbally, 2007;Jimenez et al., 2009;Poschl and Shiraiwa, 2015). A significant component of organic aerosol is secondary organic aerosol (SOA) formed from the gas phase oxidation of volatile organic compounds (VOCs) followed by partitioning of products into particles or from heterogeneous reactions of VOCs with particles (Hallquist et al., 2009;Zhang et al., 2015). Dicarboxylic acids (DCAs) are abundant and ubiquitous constituents in SOA and can be effective tracers for the oxidative processes leading to the formation of SOA (Kawamura and Ikushima, 1993;Ervens et al., 2011;Wang et al., 2012;Cheng et al., 2013). DCAs normally have high water solubility and low vapor pressure, so they play important roles in controlling the hygroscopic properties of organic aerosols (Prenni et al., 2003;Ma et al., 2013) and activating cloud condensation nuclei (Booth et al., 2009). The primary emissions of DCAs from anthropogenic sources in urban areas are minor (Huang and Yu, 2007;Stone et al., 2010), and they are mainly derived from secondary oxidation of VOCs and subsequent intermediates (Ho et al., 2010;Myriokefalitakis et al., 2011). High concentrations of DCAs have been observed in biomass burning plume (Kundu et al., 2010;Kawamura et al., 2013) with more than 70% of DCAs produced from photochemical oxidation of water-soluble organic compounds, and only a small contribution from direct biomass burning emission (van Pinxteren et al., 2014).

The production of DCAs through photochemical reactions has been reported in many field studies via the analysis of the diurnal and seasonal variations of DCA(Kawamura and Ikushima, 1993;Kawamura and Yasui, 2005;Aggarwal and Kawamura, 2008;Pavuluri et al., 2010;Ho et al., 2011;Wang et al., 2017), but the mechanism of DCAs formation is still not well understood. Oxalic acid is usually the most abundant DCA observed in the field (Kawamura et al., 2004;Ho et al., 2007;Kawamura et al., 2010). A number of ground based and airborne field studies

have found a tight correlation between oxalic acid and sulfate in ambient particles and cloud droplets, relating aqueous phase chemistry to the formation of oxalic acid in aerosols and cloud droplets (Yao et al., 2002;Yao et al., 2003;Yu et al., 2005;Sorooshian et al., 2006;Sorooshian et al., 2007a;Sorooshian et al., 2007b;Miyazaki et al., 2009;Wonaschuetz et al., 2012;Wang et al., 2016). In recent years, several model and laboratory studies suggested that the aqueous phase oxidation of highly water-soluble organics like glyoxal, methylglyoxal and glyoxylic acid can efficiently produce oxalic acid in aerosol particles and cloud droplets (Lim et al., 2010;Myriokefalitakis et al., 2011;Ervens et al., 2014;Yu et al., 2014;McNeill, 2015). Recent stable carbon isotope studies and field observations have also suggested that oxalic acid forms through aqueous phase reactions (Wang et al., 2012;Cheng et al., 2015). However, the formation process of oxalic acid in ambient aerosols is still associated with great uncertainty due to the oxidation rates of precursors and oxidant levels in photochemistry and aqueous phase chemistry, which needs to be further studied.

Online measurements of the size distribution of oxalic acid-containing particles and the mixing state of oxalic acid with other compounds in aerosols are useful to examine the formation and evolution of oxalic acid and SOA particles. Sullivan and Prather investigated the diurnal cycle and mixing state of DCA-containing particles in Asian aerosol outflow using aerosol time-of-flight mass spectrometry (ATOFMS), and proposed the formation of DCA on Asian dust (Sullivan and Prather, 2007a). In addition, Yang et al. (2009) measured oxalic acid particles in Shanghai and proposed that in-cloud processes and heterogeneous reactions on hydrated aerosols contributed to the formation of oxalic acid (Yang et al., 2009). While the formation mechanism of oxalic acid especially in urban areas is still not clear, online measurements of the mixing state of oxalic acid provide a powerful tool to better understand the formation of oxalic acid in aerosol particles and cloud droplets.

The Pearl River Delta (PRD) region has distinct meteorological seasonality under the influence of the Asian monsoon system, which brings air from the ocean in spring and summer, and carries polluted air from northern China in autumn and winter.

Strong photochemical activity occurs in summer under the condition of high temperature and relative humidity, and in winter high loadings of particles from northern cities are favorable for the occurrence of haze episode (Bi et al., 2011;Zhang et al., 2013;Zhang et al., 2014). Here we present the seasonal field measurements of the mixing state of oxalic acid-containing particles using a single particle aerosol mass spectrometer (SPAMS) in a rural supersite of the PRD region. The seasonal characteristic of oxalic acid particles and mixing state with secondary species were investigated to explore the formation mechanisms of oxalic acid and aging process of SOA.

2. Methods

2.1 Aerosol sampling

Particles were sampled using a single particle aerosol mass spectrometer (SPAMS) at the Guangdong Atmospheric Supersite (22.73N, 112.93E), a rural site at Heshan city (Figure S1). The supersite is surrounded by farm land and villages, with no local industrial or traffic emissions. Ambient aerosols were sampled to the SPAMS through a 2.5m long copper tube with 0.5m of the sampling inlet located above the top of the building. The measurement period was from July 18 to August 1 in 2014, and from January 27 to February 8 in 2015. Real-time $PM_{2.5}$ mass concentration was simultaneously measured by a TEOM monitor (series 1405, Thermo scientific), and hourly concentrations of O_3 were measured by an O_3 analyzer (model 49i, Thermo scientific). The local meteorological data including temperature, relative humidity and visibility were measured on the rooftop of the building. The average temperature during the field study was 29.5 ℃ in summer and 14.1 ℃ in winter and the average relative humidity was 71.7% and 63% in summer and winter, respectively.

2.2 SPAMS

Real-time measurements of single atmospheric particles has been demonstrated by Prather and co-workers in the 1990s using aerosol time-of-flight mass spectrometry (ATOFMS) (Prather et al., 1994;Noble and Prather, 1996). Based on the same principle, the single particle aerosol mass spectrometer (SPAMS) developed by

159 Guangzhou Hexin Analytical Company was applied to field measurements of single

160 particles in the current work. The details of the SPAMS system have been introduced

161 previously (Li et al., 2011). Briefly, aerosol particles are sampled into the vacuum

162 pumped aerodynamic lens of the SPAMS through an electro-spark machined 80μm

163 critical orifice at a flow rate of 75 ml min^{-1}. The individual particles with a terminal

164 velocity are introduced to the sizing region. The velocity of each single particle is

165 detected by two continuous laser beams (diode Nd:YAG, 532 nm) with a space of 6

166 cm. The velocity is then used to calculate the single particle aerodynamic diameter

167 and provide the precise timing of the firing of a 266 nm laser used to induce

168 desorption and ionization (Nd:YAG laser, 266nm). The energy of the

169 desorption/ionization 266 nm laser was 0.6 mJ and the power density was kept at

170 about 1.6×10^8 W/cm^2 during both sampling periods. The 266 nm laser generates

171 positive and negative ions that are detected by a Z-shaped bipolar time of flight mass

172 spectrometer. The size range of the detected single particles is 0.2 to 2 μm.

173 Polystyrene latex spheres (Nanosphere size standards, Duke Scientific Corp., Palo

174 Alto) of 0.22-2.0 μm diameter were used for size calibration.

175 **2.3 Data analysis**

176 The size and chemical composition of single particles detected by SPAMS were

177 analyzed using the COCO toolkit based on the Matlab software. Particles were

178 clustered into several groups using the neural network algorithm (ART-2a) to group

179 particles into clusters with similar mass spectrum features. The ART-2a parameters

180 used in this work were set to a vigilance factor of 0.8, a learning rate of 0.05, and a

181 maximum of 20 iterations. We collected 516,679 and 767,986 particles with both

182 positive and negative mass spectra in summer and winter respectively. A standard

183 solution of oxalic acid was prepared with pure oxalic acid ($H_2C_2O_4$, purity: 99.99%,

184 Aladdin Industrial Corporation) and atomized to aerosols. After drying through two

185 silica gel diffusion driers, pure oxalic acid particles were directly introduced into the

186 SPAMS. The positive and negative mass spectra of oxalic acid are shown in Figure S2.

187 Based on the mass spectra of pure oxalic acid and previous ambient measurements by

188 ATOFMS (Silva and Prather, 2000;Sullivan and Prather, 2007a;Yang et al., 2009),

189    $HC_2O_4^-$ (m/z -89) is selected as the ion peak for oxalic acid containing particles. In

190   this work, oxalic acid particles are identified if the peak area of m/z -89 was larger

191   than 0.5% of the total signal in the mass spectrum. With this threshold, 13109 and

192   20504 of oxalic acid-containing particles were obtained in summer and winter

193   separately, accounting for 2.5% and 2.7% of the total detected particles. The

194   percentage of oxalic acid-containing particles in total particles in this work was

195   comparable to the reported value in the urban area of Shanghai (3.4%) (Yang et al.,

196   2009). However, these percentages are in general much lower than those reported in

197   cleaner environments such as the western Pacific Ocean where oxalic acid was found

198   in up to 1-40% of total particles due to little anthropogenic influences (Sullivan and

199   Prather, 2007a).

200   The oxalic acid containing particles are classified into eight types in the

201   following order: elemental carbon (EC), organic carbon (OC), elemental and organic

202   carbon (ECOC), biomass burning (BB), heavy metal (HM), secondary (Sec),

203   sodium-potassium (NaK) and dust. Different type particles are identified according to

204   characteristic ion markers and dominant chemical species (Table S1): (1) particles

205   containing abundant carbon clusters like $\pm12[C]^{+/-}$, $\pm24[C_2]^{+/-}$, $\pm36[C_3]^{+/-}$ with relative

206   peak area more than 0.5% are classified as EC type, (2) any remaining particles

207   containing abundant signals of $27[C_2H_3]^+$, $43[C_2H_3O]^+$ and hydrocarbon clusters with

208   relative peak area more than 0.5% are classified as OC type, (3) any remaining

209   particles containing signals of $\pm12[C]^{+/-}$, $\pm24[C_2]^{+/-}$, $37[C_3H]^+$ and $43[C_2H_3O]^+$ with

210   relative peak area more than 0.5% are classified as ECOC type, (4) any remaining

211   particles containing abundant signals of $39[K]^+$ (peak area>1500) with relative peak

212   area of $-59[C_2H_3O_2]^-$ and $-73[C_3H_5O_2]^-$ simultaneously more than 0.5% are classified

213   as BB type, (5) any remaining particles containing signals of $55[Mn]^+$, $56[Fe]^+$,

214    $63/65[Cu]^+$, $64[Zn]^+$ and $208[Pb]^+$ with relative peak area more than 0.5% are

215   classified as HM type, (6) any remaining particles containing abundant signals of

216    $18[NH_4]^+$ (peak area>50), $-62[NO_3]^-$ (peak area>100) and $-97[HSO_4]^-$ (peak area>100)

217   are classified as Sec type, (7) any remaining particles containing abundant signals of

218    $23[Na]^+$ (peak area>1500) and related species are classified as NaK type, (8) any

219 remaining particles containing signals of $40[Ca]^+$, $56[CaO]^+$ and related species are

220 classified as dust type. The rules for oxalic acid particles classification in the current

221 work have been reported in previous studies (Sullivan and Prather, 2007b;Yang et al.,

222 2009;Zhang et al., 2013;Li et al., 2014).

223 **2.4 Inorganic ions and in-situ pH (pH_{is})**

224 Water-soluble inorganic ions and trace gases were determined by an online

225 analyzer for monitoring aerosols and gases (MARGA, model ADI 2080, Applikon

226 Analytical B. V. Corp., the Netherlands) with a $PM_{2.5}$ sampling inlet at one hour

227 resolution from July 18 to August 1 in 2014. The principle and instrumental design

228 has been described in detail elsewhere (ten Brink et al., 2007;Du et al., 2011;Behera et

229 al., 2013;Khezri et al., 2013). Standard solutions containing all detected ions were

230 injected into MARGA before and after the field measurement. The liquid water

231 content and the concentration of H^+ in particles are calculated using the ISORROPIA

232 II model (Nenes et al., 1998, 1999;Fountoukis and Nenes, 2007). We choose stable

233 mode and reverse type in the ISORROPIA model to calculate the concentration of H^+

234 and the liquid water content in this work. The in-situ pH (pH_{is}) of particles is

235 calculated through the following equation:

236
$$pH_{is} = -\log\alpha_{H^+} = -\log(\gamma_{H^+} \times n_{H^+} \times 1000/V_a) \tag{1}$$

237 where n_{H^+} is the concentration of H^+ (mol m^{-3}) and V_a is the volume concentration of

238 the H_2O (cm^3 m^{-3}) , while γ_{H^+} is the activity coefficient of H^+(Xue et al., 2011;Cheng

239 et al., 2015). The temporal variation of pH_{is} of ambient $PM_{2.5}$ particles is presented in

240 Figure S3, and demonstrated that 97% of particles were acidic in summer.

241 **3. Results and Discussion**

242 **3.1 Seasonal variation of oxalic acid containing particles**

243 The clustered 48 hr back trajectories of air masses arriving in Heshan during the

244 sampling period are shown in Figure S4. In summer, air masses at 500m levels above

245 the ground were mainly from the ocean and rural areas with less influence of human

246 activity, while in winter air masses were directly from urban areas of Guangzhou and

247 Foshan, indicating a strong influence from anthropogenic emissions. The temporal

248 variations of the total detected particles and oxalic acid containing particles in

249 summer and winter are shown in Figure 1. The total particles had similar trends with

250 the mass concentration of ambient $PM_{2.5}$, suggesting that the counts of total particles

251 detected by SPAMS can be representative of $PM_{2.5}$ mass concentration during the

252 whole sampling periods. The oxalic acid (C_2-containing) particles, in general,

253 exhibited distinct diurnal peaks from July 28 to August 1, while they showed different

254 temporal trends in winter. The relative abundance of oxalic acid particles in all of the

255 sampled particles (C_2/total ratio) had the same variation with the abundance of oxalic

256 acid particles in summer, especially in the period of July 28 – August 1 (Figure 1). In

257 winter, however, particle counts and relative abundance of oxalic acid had different

258 temporal changes except Jan 30 and February 5-8, when the count and relative

259 abundance of oxalic acid particles simultaneously had a sudden increase.

260 The oxalic acid-containing particles were clustered into eight groups, and they

261 altogether accounted for 89.6% and 95.1% of total oxalic acid particles in summer and

262 winter, respectively. Table 1 shows that in summer heavy metal (HM) type particles

263 contributed 31.3% to total oxalic acid particles, followed by the Sec (19.2%) and BB

264 type (13%). However, in winter BB type particles were the most abundant and

265 accounted for 24.2% of the oxalic acid-containing particles, followed by EC and HM

266 type. Besides, carbonaceous type particles including EC, OC, ECOC and BB

267 accounted for 28.1% of oxalic acid particles in summer and 59.8% in winter,

268 indicating the seasonal different characteristics of oxalic acid particles. The temporal

269 variations of eight groups of oxalic acid particles in summer and winter are illustrated

270 in Figure 1. In summer HM type particles (orange color) and total oxalic acid particles

271 exhibited similar diurnal patterns, suggesting a possible connection between the

272 production of oxalic acid and the transition metals (e.g. Fe, Cu) (Zhou et al., 2015).

273 Although Sec, BB and EC type particles showed similar diurnal patterns with total

274 oxalic acid particles, the concentrations of these type particles were generally lower

275 than HM type particles. In winter diurnal variation of oxalic acid particles was not

276 obvious but a sharp increase, accompanied by the increase of BB, EC and Sec type

277 particles, was observed on February 8.

278   The averaged positive and negative ion mass spectra of oxalic acid containing

279 particles are shown in Figure 2. The positive ion spectrum of oxalic acid particles in

280 summer was characterized by high fractions of metal ion peaks including $23[Na]^+$,

281 $27[Al]^+$, $39[K]^+$, $55[Mn]^+$, $56[Fe]^+$, $63/65[Cu]^+$, $64[Zn]^+$ and $208[Pb]^+$, and

282 carbonaceous marker ions at m/z $27[C_2H_3]^+$, $36[C_3]^+$, $43[C_2H_3O/C_3H_7]^+$, $48[C_4]^+$

283 (Figure 2 a). The negative ion spectrum of oxalic acid particles in summer was

284 characterized by the strong intensity of secondary ions including m/z $-46[NO_2]^-$,

285 $-62[NO_3]^-$, $-79[PO_3]^-$, $-80[SO_3]^-$, $-96[SO_4]^-$ and $-97[HSO_4]^-$, as well as carbon clusters

286 of $-24[C_2]^-$, $-36[C_3]^-$, $-48[C_4]^-$ and BB markers of $-59[C_2H_3O_2]^-$ and $-73[C_3H_5O_2]^-$

287 (Figure 2 b) (Zauscher et al., 2013). More carbonaceous clusters, i.e., $27[C_2H_3]^+$,

288 $29[C_2H_5]^+$, $36[C_3]^+$, $37[C_3H]^+$, $43[C_2H_3O]^+$, $48[C_4]^+$, $51[C_4H_3]^+$, $55[C_4H_7]^+$, $60[C_5]^+$,

289 $63[C_5H_3]^+$, $65[C_5H_5]^+$, $74[C_2H_2O_3]^+$, $77[C_6H_5]^+$, were observed in the positive ion

290 spectrum of oxalic acid particles in winter (Figure 2 c) than in summer. The negative

291 ion spectrum of oxalic acid particles in winter (Figure 2 d) contained a large amount

292 of secondary ions, similar to those found in summer, and a more intense signal of

293 nitric acid ($-125[HNO_3NO_3]^-$) , suggesting an acidic nature of oxalic acid particles in

294 winter.

295   The mixing state of oxalic acid particles with sulfate, nitrate and ammonium

296 (SNA) was investigated through the percentage of SNA-containing oxalic acid

297 particles in total oxalic acid particles (Figure 3). Oxalic acid was found to be

298 internally mixed with sulfate and nitrate during both sampling periods with percentage

299 of 93% and 94% in summer respectively, and both 98% in winter (Figure 3 a).

300 However, the NH_4^+-containing oxalic acid particle (C_2-NH_4^+) only accounted for 18%

301 of total oxalic acid particles in summer but this fraction increased to 71% in winter,

302 and linear correlation between C_2-NH_4^+ particles and total oxalic acid particles

303 showed better linear regression (r^2=0.98) in winter than summer, indicating a general

304 mixing state of NH_4^+ with oxalic acid in winter. Aqueous phase production of SO_4^{2-}

305 has been studied well and the linear correlation between oxalic acid and SO_4^{2-} has

306 been used to study the production of oxalic acid through aqueous phase reactions (Yu

307 et al., 2005;Miyazaki et al., 2009;Cheng et al., 2015). In our work, oxalic acid and

308 C_2-SO_4^{2-} displayed good correlations in summer and winter (both r^2=0.99), which

309 suggests a common production route of oxalic acid and sulfate, likely aqueous phase

310 reactions.

311 Figure 4 shows the unscaled size-resolved number distributions of the eight types

312 of oxalic acid particles. Oxalic acid mainly existed in 0.4 to 1.2 μm particles during

313 the entire sampling period but exhibited different peak modes for each particle type in

314 summer and winter. In summer, major types of oxalic acid particles showed distinct

315 peak mode at different size diameter. EC and Sec type particles peaked at 0.5 μm,

316 followed by BB type particles at 0.55 μm, then HM type particles at 0.6 μm, and OC

317 type particles at 0.7 μm. The difference of peak mode suggests the possible different

318 chemical evolution process for each type oxalic acid-containing particles. However, in

319 winter, oxalic acid particles showed broader size distribution from 0.5 to 0.8 μm for

320 all particle types. Oxalic acid particles of all types were generally larger in winter than

321 summer, possibly due to condensation and coagulation of particles during aging of

322 oxalic acid particles in winter.

3.2 Photochemical production of oxalic acid in summer

324 In summer oxalic acid particles showed peaks in the afternoon especially from

325 July 28 to August 1, which was in agreement with the variation pattern of the O_3

326 concentration (Figure 5), indicating a strong association of oxalic acid formation with

327 photochemical reactions. Malonic acid is another product of photochemical oxidation

328 of organic compounds (Kawamura and Ikushima, 1993;Wang et al., 2012;Meng et al.,

329 2013;Meng et al., 2014). In our campaign, malonic acid containing particles had

330 diurnal trends similar to oxalic acid particles and O_3 concentration. As the dominant

331 particle type, HM particles had identical variation pattern with total oxalic acid

332 particles. They are characterized by highly abundant metal ion peaks like 55[Mn]$^+$,

333 56[Fe]$^+$, 63/65[Cu]$^+$, 64[Zn]$^+$ and 208[Pb]$^+$, as well as secondary ion peaks of

334 -46[NO$_2$]$^-$, -62[NO$_3$]$^-$, -80[SO$_3$]$^-$, -96[SO$_4$]$^-$ and -97[HSO$_4$]$^-$ in the negative spectrum

335 in summer (Figure 6). In order to investigate the photochemical formation of oxalic

336 acid in summer, the diurnal variations of O_3, oxalic acid particles, HM type particles

337   and pH_{is} of ambient particles averaged from July 28 to August 1, 2014 are shown in

338   Figure 7. The concentration of O_3 increased after 9:00 and peaked at 17:00, while

339   oxalic acid particles and HM type particles both increased after 10:00 and showed two

340   peaks at 15:00 and 19:00. The pH_{is} of ambient particles ranging from -1.42 to 4.01

341   indicated an acidic environment, and the temporal trends of RH, inorganic ions and

342   H^+ (aq) in aerosols are shown in Figure S5. The oxidation of glyoxal and glyoxylic

343   acid by •OH has been identified as an important pathway of oxalic acid production by

344   field and laboratory studies (Ervens et al., 2004;Ervens and Volkamer, 2010;Wang et

345   al., 2012;Wang et al., 2015). In summer strong photochemical activity and high O_3

346   concentrations in the afternoon lead to more production of dicarbonyls and aldehydes

347   (e.g. glyoxal and methylglyoxal) from VOCs (Myriokefalitakis et al., 2011), which

348   increases the precursors of oxalic acid. The aqueous phase oxidation of glyoxal can

349   take place in both clouds and wet aerosols (Lim et al., 2010). However, the lower

350   yield of oxalic acid from glyoxal in wet aerosols compared to in clouds has been

351   reported in previous chamber experiments due to the formation of substantial amount

352   of high molecular weight products such as oligomers in aerosol-related concentrations

353   (Carlton et al., 2007;Tan et al., 2009). These findings may explain the lower peak of

354   oxalic acid particles at 15:00 compared to that at 19:00. Besides, the precursors of

355   oxalic acid such as glyoxylic acid have higher reaction rate with •OH in high pH

356   solutions according to previous studies(Ervens et al., 2003;Herrmann, 2003;Cheng et

357   al., 2015), and in this work the increase of pH_{is} was observed as the enhancement of

358   oxalic acid particles in the afternoon (Figure 7), which suggests an efficient oxalic

359   acid production from the oxidation of precursors.

360   The similar photochemical pattern of HM type particles with O_3 and total oxalic

361   acid particles implies a possible participation of metal ions in the formation process of

362   oxalic acid. The modeling studies from Ervens et al. (2014) suggest that oxalic acid

363   production from glyoxal and glyoxylic acid in aqueous phase significantly depends on

364   •OH availability (Ervens et al., 2014). The main sources of aqueous phase •OH in

365   cloud droplets include direct uptake from the gas phase (Jacob, 1986), ozone

366   photolysis by UV and visible light at the air-water interface (Anglada et al., 2014),

367 and also aqueous phase chemical reactions(Gligorovski et al., 2015). For the last kind

368 of source, •OH radicals could be generated through Fenton or Fenton like reactions

369 and photolysis of H_2O_2, NO_3^-, NO_2^-, and chromophoric dissolved organic matter

370 (CDOM) (Badali et al., 2015;Ervens, 2015;Herrmann et al., 2015;Tong et al., 2016).

371 Given that SPAMS cannot be used to quantify the concentrations of iron ions and

372 H_2O_2, we will investigate the relative contribution of different source •OH radicals to

373 the formation of oxalic acid and show results in our follow up studies.

374   The oxalic acid loss through the photolysis of iron oxalato complexes is a

375 significant sink according to field measurements and model simulations (Sorooshian

376 et al., 2013;Weller et al., 2014;Zhou et al., 2015). Considering the high abundance of

377 iron in oxalic acid particles in the current work (Figure 6), the photolysis of iron

378 oxalato complexes could have played an important role in the diurnal variation of

379 oxalic acid particles. Because the mass concentration of Fe (III) and oxalic acid could

380 not be obtained through SPAMS, the diurnal variations of peak area of iron (m/z=56)

381 and oxalic acid (m/z=-89) were used to investigate the role of iron on the net

382 production of oxalic in the HM type particles from July 28 to August 1, 2014 (Figure

383 8). Interestingly, the peak area of iron exhibited opposite trend with the peak area of

384 oxalic acid from 4:00 to 11:00. As the peak area of Fe increased from 1565 to 29920

385 from 4:00 to 7:00, the peak area of oxalic decreased from 6052 to 3487 accordingly.

386 From 8:00 to 11:00, the peak area of Fe had a very low value of 1168, but the peak

387 area of oxalic had a very high value of 5538. In addition, the peak area of iron

388 exhibited a high value of 138199 at 14:00, while the peak area of oxalic acid showed a

389 lower peak of 7687 at 14:00 and a higher peak of 11879 at 19:00 with an extremely

390 low abundance of iron. Above opposite variation patterns of iron and oxalic acid in

391 iron rich HM type particles during the photochemical activity period from 5:00 to

392 19:00 strongly indicated that photolysis of iron oxalato complexes could be an

393 efficient sink of oxalic acid.

394   The influence from traffic emission was investigated through the diurnal

395 variations of total EC type particles and NO_2 (Figure S6). The EC type particles

396 increased from 12:00 to 21:00, which had same variation as total oxalic acid, but NO_2

397 followed the rush hour pattern with two peaks from 5:00 to 8:00 and from 18:00 to

398 21:00. Traffic emission is not expected to have a large contribution to oxalic acid in

399 this study. The wind speed was low during the whole day (Figure S6), especially

400 between 9:00 and 18:00, which provided a stagnant environment for the increase in

401 oxalic acid produced from photochemical process.

3.3 Formation process of oxalic acid in winter

403 Despite lower O_3 concentrations and photochemical activity in winter, oxalic

404 acid was still prevalent in carbonaceous particles, especially BB type particles. While

405 oxalic acid was found to be internally mixed with sulfate and nitrate both in summer

406 and winter, the nitric acid was only observed in oxalic acid particles in winter,

407 indicating a strongly acidic nature of oxalic acid particles in winter. Considering a

408 possible connection of oxalic acid production with the acidic environment, the

409 temporal concentrations of oxalic acid, sulfate and nitrate were investigated through

410 their peak areas in the carbonaceous type oxalic acid particles including EC, OC,

411 ECOC and BB type in Figure 9. The peaks of m/z -62[NO_3]$^-$ and - 97[HSO_4]$^-$

412 represent nitrate and sulfate, respectively. Nitrate, sulfate and oxalic acid showed very

413 similar variation patterns in winter, suggesting a close connection of the formation of

414 oxalic acid with the existence of nitrate and sulfate. Although nitric acid was found in

415 the oxalic acid particles, the acidity of the oxalic acid particles was not estimated

416 since the real-time concentration of inorganic ions was not available during the

417 sampling period in winter. Instead the relative acidity ratio (R_{ra}), defined as the ratio

418 of total peak areas of nitrate and sulfate to the peak area of ammonium (m/z

419 18[NH_4]$^+$), was used (Denkenberger et al., 2007;Pratt et al., 2009). The R_{ra} of

420 carbonaceous type oxalic acid particles ranged from 7 to 114 with an average value of

421 25 (Figure 9), indicating an intensely acidic environment of carbonaceous type oxalic

422 acid particles in winter. Several studies have reported the formation of oxalic acid

423 through the oxidation of glyoxal and related precursors in acidic aqueous phase

424 (Carlton et al., 2006;Carlton et al., 2007;Tan et al., 2009). Although the influence of

425 different particle acidity on the oxidation process of glyoxal still needs evaluation, the

426 moderate acidic environment is favorable for the production of oxalic acid from the

427 oxidation of glyoxal (Herrmann, 2003;Ervens and Volkamer, 2010;Eugene et al.,

428 2016). In this work the acidic environment of the carbonaceous type oxalic acid

429 particles and similar variation patterns among oxalic acid, sulfate and nitrate may

430 suggest a relationship between the degradation of organic precursors and the acidic

431 chemical process. However, the temporal change of R_{ra} did not follow a similar trend

432 as the peak area of oxalic acid in most particles, possibly due to the multi-step

433 formation of oxalic acid influenced by many factors such as precursors, liquid water

434 content and ion strength (Carlton et al., 2007;Cheng et al., 2013;Cheng et al., 2015).

435 The sharp increase of oxalic acid particles on February 8, 2015 (Figure 1) was

436 selected as a typical episode to investigate the formation processes of oxalic acid in

437 winter. During the episode, the 48 hr back trajectory analysis showed air masses that

438 originated from the urban areas of Guangzhou and Foshan city (Figure S4), indicating

439 strong influence on organic precursors from anthropogenic emissions. Oxalic acid

440 particle types were dominated by BB (23.2%), followed by EC (22.0%) and Sec

441 (15.1%) type (Table 2). Carbonaceous particles including EC, ECOC, OC, BB

442 accounted for 61.6% of the total oxalic acid particles. The mass spectra of oxalic acid

443 particles were characterized by many hydrocarbon clusters of $27[C_2H_3]^+$, $29[C_2H_5]^+$,

444 $37[C_3H]^+$, $43[C_2H_3O]^+$, $51[C_4H_3]^+$, $55[C_4H_7]^+$, $63[C_5H_3]^+$, $65[C_5H_5]^+$, $74[C_2H_2O_3]^+$,

445 $77[C_6H_5]^+$, and carbon clusters of $36[C_3]^+$, $48[C_4]^+$, $60[C_5]^+$ in positive mass spectrum,

446 while the negative mass spectrum was characterized by elemental carbon clusters like

447 $-24[C_2]^-$, $-36[C_3]^-$, $-48[C_4]^-$, biomass burning markers of $-59[C_2H_3O_2]^-$ and

448 $-73[C_3H_5O_2]^-$ and secondary species including $-42[CNO]^-$, $-46[NO_2]^-$, $-62[NO_3]^-$,

449 $-79[PO_3]^-$, $-80[SO_3]^-$, $-96[SO_4]^-$ and $-97[HSO_4]^-$ (Figure 10 a).

450 As the precursor of oxalic acid, glyoxal has the potential to react with sulfuric

451 acid to produce organosulfates through acid-catalyzed nucleophilic addition according

452 to laboratory and chamber studies(Surratt et al., 2007;Galloway et al., 2009). The

453 negative ion of $-155([C_2H_3O_2SO_4]^-)$ has been identified as the marker ion of

454 organosulfates derived from glyoxal in chamber and field measurements using

455 ATOFMS (Surratt et al., 2008;Hatch et al., 2011). The formation of organosulfates

456 from glyoxal requires an acidic aqueous environment, which can be used as a marker

of acidic aqueous phase aging process of organic compounds. The temporal trend of organosulfate-containing oxalic acid particles in winter is shown in Figure S7, which exhibited a similar pattern as the total oxalic acid particles during the whole sampling period in winter. The percentage of organosulfate-containing oxalic acid particles in total oxalic acid particles ranged from 0 to 16.4% with the highest ratio observed in the episode (February 8). The linear regression between total oxalic acid particles and organosulfate-containing oxalic acid particles in the episode is exhibited in Figure 10b, and the robust correlation (r^2=0.81) between them suggests that oxalic acid and organosulfate may share similar formation process. Based on the above discussion, the degradation of carbonaceous species associated with acidic aqueous phase chemical reactions may have an important contribution to the formation of oxalic acid during the episode in winter. Similar particle types and mass spectra of oxalic acid-containing particles during the episode and the whole sampling period in winter were observed, which suggests the acidic aqueous phase chemical processing of organic precursors as a potential source for oxalic acid.

4. Summary and conclusions

Oxalic acid containing particles were measured by a single particle aerosol mass spectrometer (SPAMS) in the summer and winter of 2014 in Heshan, China. They accounted for 2.5% and 2.7% of the total detected ambient particles. In summer heavy metal-containing particles were the largest group of particles containing oxalic acid with a fraction of 31.3% followed by Sec type (19.2%), while in winter BB type was the dominant group with a percentage of 24.2%. More than 90% of oxalic acid particles were internally mixed with sulfate and nitrate during the whole sampling period. Only 18% of oxalic acid particles contained ammonium in summer, which increased to 71% in winter. In summer oxalic acid and O_3 concentration exhibited similar diurnal variations, indicating a substantial contribution of photochemical reactions to oxalic acid formation. The diurnal variations of peak area of iron and oxalic acid in HM type particles indicate a net production of oxalic acid at 15:00 lower than at 19:00, likely due to a significant loss of oxalic acid through the

photolysis of iron oxalato complexes during the strong photochemical activity period. In winter carbonaceous type particles including EC, OC, ECOC and BB groups accounted for 59.8% of oxalic acid particles and increased to 61.6% in the episode. Nitric acid and organosulfate were found to co-exist in oxalic acid-containing particles in the winter, which suggests a close association with acidic aqueous phase reactions. Acidic aqueous phase chemical processing of organic precursors is a potential contribution for the formation of oxalic acid in winter. The current study demonstrates that SPAMS is a unique tool for understanding the mixing states of different components of ambient aerosols, which are useful for exploring the formation and evolution process of SOA.

Acknowledgements

This work was financially supported by National Key Technology R&D Program (Grant No. 2014BAC21B01), Guangdong Province Public Interest Research and Capacity Building Special Fund (Grant No. 2014B020216005), the Strategic Priority Research Program (B) of the Chinese Academy of Sciences (Grant No. XDB05040502), Guangdong Industry-University Research Program (Grant No.2012B090500014), and NSFC of Guangdong Province (Grant No. 2015A030313339). Chak K. Chan would like to acknowledge funding support of the General Fund of National Natural Science Foundation of China (Grant No. 41675117). Haijie Tong acknowledge Max Planck Society for funding and Ulrich Pöschl for helpful discussions.

References

Aggarwal, S. G., and Kawamura, K.: Molecular distributions and stable carbon isotopic compositions of dicarboxylic acids and related compounds in aerosols from Sapporo, Japan: Implications for photochemical aging during long-range atmospheric transport, Journal of Geophysical Research-Atmospheres, 113, D14301, 10.1029/2007jd009365, 2008.

Anglada, J. M., Martins-Costa, M., Ruiz-López, M. F., and Francisco, J. S.: Spectroscopic signatures of ozone at the air–water interface and photochemistry implications, Proceedings of the National Academy of Sciences, 111, 11618-11623, 10.1073/pnas.1411727111, 2014.

Badali, K. M., Zhou, S., Aljawhary, D., Antinolo, M., Chen, W. J., Lok, A., Mungall, E., Wong, J. P. S., Zhao, R., and Abbatt, J. P. D.: Formation of hydroxyl radicals from photolysis of secondary organic aerosol material, Atmospheric Chemistry and Physics, 15, 7831-7840,

518   10.5194/acp-15-7831-2015, 2015.

519   Behera, S. N., Betha, R., Liu, P., and Balasubramanian, R.: A study of diurnal variations of PM 2.5
520   acidity and related chemical species using a new thermodynamic equilibrium model, Science of
521   the Total Environment, 452, 286-295, 2013.

522   Bi, X., Zhang, G., Li, L., Wang, X., Li, M., Sheng, G., Fu, J., and Zhou, Z.: Mixing state of biomass
523   burning particles by single particle aerosol mass spectrometer in the urban area of PRD, China,
524   Atmospheric Environment, 45, 3447-3453, 2011.

525   Booth, A. M., Topping, D. O., McFiggans, G., and Percival, C. J.: Surface tension of mixed inorganic
526   and dicarboxylic acid aqueous solutions at 298.15 K and their importance for cloud activation
527   predictions, Phys Chem Chem Phys, 11, 8021-8028, 10.1039/b906849j, 2009.

528   Carlton, A. G., Turpin, B. J., Lim, H. J., Altieri, K. E., and Seitzinger, S.: Link between isoprene and
529   secondary organic aerosol (SOA): Pyruvic acid oxidation yields low volatility organic acids in
530   clouds, Geophysical Research Letters, 33, L06822, 10.1029/2005gl025374, 2006.

531   Carlton, A. G., Turpin, B. J., Altieri, K. E., Seitzinger, S., Reff, A., Lim, H. J., and Ervens, B.:
532   Atmospheric oxalic acid and SOA production from glyoxal: Results of aqueous photooxidation
533   experiments, Atmospheric Environment, 41, 7588-7602, 10.1016/j.atmosenv.2007.05.035, 2007.

534   Cheng, C., Wang, G., Meng, J., Wang, Q., Cao, J., Li, J., and Wang, J.: Size-resolved airborne
535   particulate oxalic and related secondary organic aerosol species in the urban atmosphere of
536   Chengdu, China, Atmospheric Research, 161, 134-142, 2015.

537   Cheng, C. L., Wang, G. H., Zhou, B. H., Meng, J. J., Li, J. J., Cao, J. J., and Xiao, S.: Comparison of
538   dicarboxylic acids and related compounds in aerosol samples collected in Xi'an, China during haze
539   and clean periods, Atmospheric Environment, 81, 443-449, 10.1016/j.atmosenv.2013.09.013,
540   2013.

541   Denkenberger, K. A., Moffet, R. C., Holecek, J. C., Rebotier, T. P., and Prather, K. A.: Real-time,
542   single-particle measurements of oligomers in aged ambient aerosol particles, Environmental
543   Science & Technology, 41, 5439-5446, 10.1021/es070329l, 2007.

544   Du, H., Kong, L., Cheng, T., Chen, J., Du, J., Li, L., Xia, X., Leng, C., and Huang, G.: Insights into
545   summertime haze pollution events over Shanghai based on online water-soluble ionic composition
546   of aerosols, Atmospheric Environment, 45, 5131-5137, 2011.

547   Ervens, B., Gligorovski, S., and Herrmann, H.: Temperature-dependent rate constants for hydroxyl
548   radical reactions with organic compounds in aqueous solutions, Phys Chem Chem Phys, 5,
549   1811-1824, Doi 10.1039/B300072a, 2003.

550   Ervens, B., Feingold, G., Frost, G. J., and Kreidenweis, S. M.: A modeling study of aqueous production
551   of dicarboxylic acids: 1. Chemical pathways and speciated organic mass production, Journal of
552   Geophysical Research-Atmospheres, 109, D15205, 10.1029/2003jd004387, 2004.

553   Ervens, B., and Volkamer, R.: Glyoxal processing by aerosol multiphase chemistry: towards a kinetic
554   modeling framework of secondary organic aerosol formation in aqueous particles, Atmospheric
555   Chemistry and Physics, 10, 8219-8244, DOI 10.5194/acp-10-8219-2010, 2010.

556   Ervens, B., Turpin, B. J., and Weber, R. J.: Secondary organic aerosol formation in cloud droplets and
557   aqueous particles (aqSOA): a review of laboratory, field and model studies, Atmospheric
558   Chemistry and Physics, 11, 11069-11102, 10.5194/acp-11-11069-2011, 2011.

559   Ervens, B., Sorooshian, A., Lim, Y. B., and Turpin, B. J.: Key parameters controlling OH-initiated
560   formation of secondary organic aerosol in the aqueous phase (aqSOA), Journal of Geophysical
561   Research-Atmospheres, 119, 3997-4016, 10.1002/2013JD021021, 2014.

Ervens, B.: Modeling the Processing of Aerosol and Trace Gases in Clouds and Fogs, Chem Rev, 115, 4157-4198, 10.1021/cr5005887, 2015.

Eugene, A. J., Xia, S. S., and Guzman, M. I.: Aqueous Photochemistry of Glyoxylic Acid, Journal of Physical Chemistry A, 120, 3817-3826, 10.1021/acs.jpca.6b00225, 2016.

Fountoukis, C., and Nenes, A.: ISORROPIA II: a computationally efficient thermodynamic equilibrium model for K+–Ca 2+–Mg 2+–NH 4+–Na+–SO 4 2−–NO 3−–Cl−–H 2 O aerosols, Atmospheric Chemistry and Physics, 7, 4639-4659, 2007.

Galloway, M. M., Chhabra, P. S., Chan, A. W. H., Surratt, J. D., Flagan, R. C., Seinfeld, J. H., and Keutsch, F. N.: Glyoxal uptake on ammonium sulphate seed aerosol: reaction products and reversibility of uptake under dark and irradiated conditions, Atmospheric Chemistry and Physics, 9, 3331-3345, 10.5194/acp-9-3331-2009, 2009.

Gligorovski, S., Strekowski, R., Barbati, S., and Vione, D.: Environmental Implications of Hydroxyl Radicals (•OH), Chem Rev, 115, 13051-13092, 10.1021/cr500310b, 2015.

Goldstein, A. H., and Galbally, I. E.: Known and unexplored organic constituents in the earth's atmosphere, Environmental Science & Technology, 41, 1514-1521, Doi 10.1021/Es072476p, 2007.

Hallquist, M., Wenger, J. C., Baltensperger, U., Rudich, Y., Simpson, D., Claeys, M., Dommen, J., Donahue, N. M., George, C., Goldstein, A. H., Hamilton, J. F., Herrmann, H., Hoffmann, T., Iinuma, Y., Jang, M., Jenkin, M. E., Jimenez, J. L., Kiendler-Scharr, A., Maenhaut, W., McFiggans, G., Mentel, T. F., Monod, A., Prévôt, A. S. H., Seinfeld, J. H., Surratt, J. D., Szmigielski, R., and Wildt, J.: The formation, properties and impact of secondary organic aerosol: current and emerging issues, Atmospheric Chemistry and Physics, 9, 5155-5236, 10.5194/acp-9-5155-2009, 2009.

Hatch, L. E., Creamean, J. M., Ault, A. P., Surratt, J. D., Chan, M. N., Seinfeld, J. H., Edgerton, E. S., Su, Y., and Prather, K. A.: Measurements of isoprene-derived organosulfates in ambient aerosols by aerosol time-of-flight mass spectrometry-Part 1: Single particle atmospheric observations in Atlanta, Environmental science & technology, 45, 5105-5111, 2011.

Herrmann, H.: Kinetics of aqueous phase reactions relevant for atmospheric chemistry, Chem Rev, 103, 4691-4716, Doi 10.1021/Cr020658q, 2003.

Herrmann, H., Schaefer, T., Tilgner, A., Styler, S. A., Weller, C., Teich, M., and Otto, T.: Tropospheric Aqueous-Phase Chemistry: Kinetics, Mechanisms, and Its Coupling to a Changing Gas Phase, Chem Rev, 115, 4259-4334, 10.1021/cr500447k, 2015.

Ho, K. F., Cao, J. J., Lee, S. C., Kawamura, K., Zhang, R. J., Chow, J. C., and Watson, J. G.: Dicarboxylic acids, ketocarboxylic acids, and dicarbonyls in the urban atmosphere of China, Journal of Geophysical Research-Atmospheres, 112, D22S27, 10.1029/2006jd008011, 2007.

Ho, K. F., Lee, S. C., Ho, S. S. H., Kawamura, K., Tachibana, E., Cheng, Y., and Zhu, T.: Dicarboxylic acids, ketocarboxylic acids, alpha-dicarbonyls, fatty acids, and benzoic acid in urban aerosols collected during the 2006 Campaign of Air Quality Research in Beijing (CAREBeijing-2006), Journal of Geophysical Research-Atmospheres, 115, D19312, 10.1029/2009jd013304, 2010.

Ho, K. F., Ho, S. S. H., Lee, S. C., Kawamura, K., Zou, S. C., Cao, J. J., and Xu, H. M.: Summer and winter variations of dicarboxylic acids, fatty acids and benzoic acid in PM(2.5) in Pearl Delta River Region, China, Atmospheric Chemistry and Physics, 11, 2197-2208, 10.5194/acp-11-2197-2011, 2011.

Huang, X.-F., and Yu, J. Z.: Is vehicle exhaust a significant primary source of oxalic acid in ambient

606   aerosols?, Geophysical Research Letters, 34, L02808, 10.1029/2006gl028457, 2007.

607   Jacob, D. J.: Chemistry of OH in remote clouds and its role in the production of formic acid and

608   peroxymonosulfate, Journal of Geophysical Research: Atmospheres, 91, 9807-9826,

609   10.1029/JD091iD09p09807, 1986.

610   Jimenez, J. L., Canagaratna, M. R., Donahue, N. M., Prevot, A. S. H., Zhang, Q., Kroll, J. H., DeCarlo,

611   P. F., Allan, J. D., Coe, H., Ng, N. L., Aiken, A. C., Docherty, K. S., Ulbrich, I. M., Grieshop, A. P.,

612   Robinson, A. L., Duplissy, J., Smith, J. D., Wilson, K. R., Lanz, V. A., Hueglin, C., Sun, Y. L.,

613   Tian, J., Laaksonen, A., Raatikainen, T., Rautiainen, J., Vaattovaara, P., Ehn, M., Kulmala, M.,

614   Tomlinson, J. M., Collins, D. R., Cubison, M. J., Dunlea, E. J., Huffman, J. A., Onasch, T. B.,

615   Alfarra, M. R., Williams, P. I., Bower, K., Kondo, Y., Schneider, J., Drewnick, F., Borrmann, S.,

616   Weimer, S., Demerjian, K., Salcedo, D., Cottrell, L., Griffin, R., Takami, A., Miyoshi, T.,

617   Hatakeyama, S., Shimono, A., Sun, J. Y., Zhang, Y. M., Dzepina, K., Kimmel, J. R., Sueper, D.,

618   Jayne, J. T., Herndon, S. C., Trimborn, A. M., Williams, L. R., Wood, E. C., Middlebrook, A. M.,

619   Kolb, C. E., Baltensperger, U., and Worsnop, D. R.: Evolution of Organic Aerosols in the

620   Atmosphere, Science, 326, 1525-1529, 10.1126/science.1180353, 2009.

621   Kawamura, K., and Ikushima, K.: seasonal-changes in the distribution of dicarboxylic-acids in the

622   urban atmosphere, Environmental Science & Technology, 27, 2227-2235, 10.1021/es00047a033,

623   1993.

624   Kawamura, K., Kobayashi, M., Tsubonuma, N., Mochida, M., Watanabe, T., and Lee, M.: Organic and

625   inorganic compositions of marine aerosols from East Asia: Seasonal variations of water-soluble

626   dicarboxylic acids, major ions, total carbon and nitrogen, and stable C and N isotopic composition,

627   Geochemical Investigations in Earth and Space Science: A Tribute to Issac R. Kaplan, 9, edited by:

628   Hill, R. J. L. J. A. Z. B. M. J. C. G., and Eganhouse, R. G. M. P. K., 243-265 pp., 2004.

629   Kawamura, K., and Yasui, O.: Diurnal changes in the distribution of dicarboxylic acids, ketocarboxylic

630   acids and dicarbonyls in the urban Tokyo atmosphere, Atmospheric Environment, 39, 1945-1960,

631   10.1016/j.atmosenv.2004.12.014, 2005.

632   Kawamura, K., Kasukabe, H., and Barrie, L. A.: Secondary formation of water-soluble organic acids

633   and alpha-dicarbonyls and their contributions to total carbon and water-soluble organic carbon:

634   Photochemical aging of organic aerosols in the Arctic spring, Journal of Geophysical

635   Research-Atmospheres, 115, D21306, 10.1029/2010jd014299, 2010.

636   Kawamura, K., Tachibana, E., Okuzawa, K., Aggarwal, S. G., Kanaya, Y., and Wang, Z. F.: High

637   abundances of water-soluble dicarboxylic acids, ketocarboxylic acids and alpha-dicarbonyls in the

638   mountaintop aerosols over the North China Plain during wheat burning season, Atmospheric

639   Chemistry and Physics, 13, 8285-8302, 10.5194/acp-13-8285-2013, 2013.

640   Khezri, B., Mo, H., Yan, Z., Chong, S.-L., Heng, A. K., and Webster, R. D.: Simultaneous online

641   monitoring of inorganic compounds in aerosols and gases in an industrialized area, Atmospheric

642   Environment, 80, 352-360, 2013.

643   Kundu, S., Kawamura, K., Andreae, T. W., Hoffer, A., and Andreae, M. O.: Molecular distributions of

644   dicarboxylic acids, ketocarboxylic acids and alpha-dicarbonyls in biomass burning aerosols:

645   implications for photochemical production and degradation in smoke layers, Atmospheric

646   Chemistry and Physics, 10, 2209-2225, 10.5194/acp-10-2209-2010, 2010.

647   Li, L., Huang, Z. X., Dong, J. G., Li, M., Gao, W., Nian, H. Q., Fu, Z., Zhang, G. H., Bi, X. H., Cheng,

648   P., and Zhou, Z.: Real time bipolar time-of-flight mass spectrometer for analyzing single aerosol

649   particles, Int J Mass Spectrom, 303, 118-124, 10.1016/j.ijms.2011.01.017, 2011.

Li, L., Li, M., Huang, Z., Gao, W., Nian, H., Fu, Z., Gao, J., Chai, F., and Zhou, Z.: Ambient particle characterization by single particle aerosol mass spectrometry in an urban area of Beijing, Atmospheric Environment, 94, 323-331, 2014.

Lim, Y. B., Tan, Y., Perri, M. J., Seitzinger, S. P., and Turpin, B. J.: Aqueous chemistry and its role in secondary organic aerosol (SOA) formation, Atmospheric Chemistry and Physics, 10, 10521-10539, 10.5194/acp-10-10521-2010, 2010.

Ma, Q. X., He, H., and Liu, C.: Hygroscopic properties of oxalic acid and atmospherically relevant oxalates, Atmospheric Environment, 69, 281-288, 10.1016/j.atmosenv.2012.12.011, 2013.

McNeill, V. F.: Aqueous organic chemistry in the atmosphere: Sources and chemical processing of organic aerosols, Environmental science & technology, 49, 1237-1244, 2015.

Meng, J. J., Wang, G. H., Li, J. J., Cheng, C. L., and Cao, J. J.: Atmospheric oxalic acid and related secondary organic aerosols in Qinghai Lake, a continental background site in Tibet Plateau, Atmospheric Environment, 79, 582-589, 10.1016/j.atmosenv.2013.07.024, 2013.

Meng, J. J., Wang, G. H., Li, J. J., Cheng, C. L., Ren, Y. Q., Huang, Y., Cheng, Y. T., Cao, J. J., and Zhang, T.: Seasonal characteristics of oxalic acid and related SOA in the free troposphere of Mt. Hua, central China: Implications for sources and formation mechanisms, Science Of The Total Environment, 493, 1088-1097, 10.1016/j.scitotenv.2014.04.086, 2014.

Miyazaki, Y., Aggarwal, S. G., Singh, K., Gupta, P. K., and Kawamura, K.: Dicarboxylic acids and water-soluble organic carbon in aerosols in New Delhi, India, in winter: Characteristics and formation processes, Journal of Geophysical Research-Atmospheres, 114, D19206, 10.1029/2009jd011790, 2009.

Myriokefalitakis, S., Tsigaridis, K., Mihalopoulos, N., Sciare, J., Nenes, A., Kawamura, K., Segers, A., and Kanakidou, M.: In-cloud oxalate formation in the global troposphere: a 3-D modeling study, Atmospheric Chemistry and Physics, 11, 5761-5782, 10.5194/acp-11-5761-2011, 2011.

Nenes, A., Pandis, S. N., and Pilinis, C.: ISORROPIA: A new thermodynamic equilibrium model for multiphase multicomponent inorganic aerosols, Aquatic geochemistry, 4, 123-152, 1998.

Nenes, A., Pandis, S. N., and Pilinis, C.: Continued development and testing of a new thermodynamic aerosol module for urban and regional air quality models, Atmospheric Environment, 33, 1553-1560, 1999.

Noble, C. A., and Prather, K. A.: Real-time measurement of correlated size and composition profiles of individual atmospheric aerosol particles, Environmental science & technology, 30, 2667-2680, 1996.

Novakov, T., and Penner, J. E.: Large Contribution of Organic Aerosols to Cloud-Condensation-Nuclei Concentrations, Nature, 365, 823-826, Doi 10.1038/365823a0, 1993.

Pavuluri, C. M., Kawamura, K., and Swaminathan, T.: Water-soluble organic carbon, dicarboxylic acids, ketoacids, and alpha-dicarbonyls in the tropical Indian aerosols, Journal of Geophysical Research-Atmospheres, 115, D11302, 10.1029/2009JD012661, 2010.

Poschl, U., and Shiraiwa, M.: Multiphase Chemistry at the Atmosphere-Biosphere Interface Influencing Climate and Public Health in the Anthropocene, Chem Rev, 115, 4440-4475, 10.1021/cr500487s, 2015.

Prather, K. A., Nordmeyer, T., and Salt, K.: Real-time characterization of individual aerosol particles using time-of-flight mass spectrometry, Anal. Chem., 66, 1403-1407, 1994.

Pratt, K. A., Hatch, L. E., and Prather, K. A.: Seasonal Volatility Dependence of Ambient Particle Phase Amines, Environmental Science & Technology, 43, 5276-5281, 10.1021/es803189n, 2009.

694   Prenni, A. J., De Mott, P. J., and Kreidenweis, S. M.: Water uptake of internally mixed particles
695   containing ammonium sulfate and dicarboxylic acids, Atmospheric Environment, 37, 4243-4251,
696   10.1016/s1352-2310(03)00559-4, 2003.

697   Silva, P. J., and Prather, K. A.: Interpretation of mass spectra from organic compounds in aerosol
698   time-of-flight mass spectrometry, Anal. Chem., 72, 3553-3562, 2000.

699   Sorooshian, A., Varutbangkul, V., Brechtel, F. J., Ervens, B., Feingold, G., Bahreini, R., Murphy, S. M.,
700   Holloway, J. S., Atlas, E. L., Buzorius, G., Jonsson, H., Flagan, R. C., and Seinfeld, J. H.: Oxalic
701   acid in clear and cloudy atmospheres: Analysis of data from International Consortium for
702   Atmospheric Research on Transport and Transformation 2004, Journal of Geophysical
703   Research-Atmospheres, 111, 10.1029/2005jd006880, 2006.

704   Sorooshian, A., Lu, M.-L., Brechtel, F. J., Jonsson, H., Feingold, G., Flagan, R. C., and Seinfeld, J. H.:
705   On the source of organic acid aerosol layers above clouds, Environmental Science & Technology,
706   41, 4647-4654, 10.1021/es0630442, 2007a.

707   Sorooshian, A., Ng, N. L., Chan, A. W. H., Feingold, G., Flagan, R. C., and Seinfeld, J. H.: Particulate
708   organic acids and overall water-soluble aerosol composition measurements from the 2006 Gulf of
709   Mexico Atmospheric Composition and Climate Study (GoMACCS), Journal of Geophysical
710   Research-Atmospheres, 112, 10.1029/2007jd008537, 2007b.

711   Sorooshian, A., Wang, Z., Coggon, M. M., Jonsson, H. H., and Ervens, B.: Observations of Sharp
712   Oxalate Reductions in Stratocumulus Clouds at Variable Altitudes: Organic Acid and Metal
713   Measurements During the 2011 E-PEACE Campaign, Environmental Science & Technology, 47,
714   7747-7756, 10.1021/es4012383, 2013.

715   Stone, E. A., Hedman, C. J., Zhou, J. B., Mieritz, M., and Schauer, J. J.: Insights into the nature of
716   secondary organic aerosol in Mexico City during the MILAGRO experiment 2006, Atmospheric
717   Environment, 44, 312-319, 10.1016/j.atmosenv.2009.10.036, 2010.

718   Sullivan, R. C., and Prather, K. A.: Investigations of the diurnal cycle and mixing state of oxalic acid in
719   individual particles in Asian aerosol outflow, Environmental Science & Technology, 41,
720   8062-8069, 10.1021/es071134g, 2007a.

721   Sullivan, R. C., and Prather, K. A.: Investigations of the diurnal cycle and mixing state of oxalic acid in
722   individual particles in Asian aerosol outflow, Environmental Science Technology, 41, 8062-8069,
723   2007b.

724   Surratt, J. D., Kroll, J. H., Kleindienst, T. E., Edney, E. O., Claeys, M., Sorooshian, A., Ng, N. L.,
725   Offenberg, J. H., Lewandowski, M., Jaoui, M., Flagan, R. C., and Seinfeld, J. H.: Evidence for
726   organosulfates in secondary organic aerosol, Environmental Science & Technology, 41, 517-527,
727   10.1021/Es062081q, 2007.

728   Surratt, J. D., Gomez-Gonzalez, Y., Chan, A. W. H., Vermeylen, R., Shahgholi, M., Kleindienst, T. E.,
729   Edney, E. O., Offenberg, J. H., Lewandowski, M., Jaoui, M., Maenhaut, W., Claeys, M., Flagan, R.
730   C., and Seinfeld, J. H.: Organosulfate formation in biogenic secondary organic aerosol, Journal of
731   Physical Chemistry A, 112, 8345-8378, Doi 10.1021/Jp802310p, 2008.

732   Tan, Y., Perri, M. J., Seitzinger, S. P., and Turpin, B. J.: Effects of Precursor Concentration and Acidic
733   Sulfate in Aqueous Glyoxal-OH Radical Oxidation and Implications for Secondary Organic
734   Aerosol, Environmental Science & Technology, 43, 8105-8112, 10.1021/Es901742f, 2009.

735   ten Brink, H., Otjes, R., Jongejan, P., and Slanina, S.: An instrument for semi-continuous monitoring of
736   the size-distribution of nitrate, ammonium, sulphate and chloride in aerosol, Atmospheric
737   Environment, 41, 2768-2779, 2007.

738 Tong, H. J., Arangio, A. M., Lakey, P. S. J., Berkemeier, T., Liu, F. B., Kampf, C. J., Brune, W. H.,
739   Poschl, U., and Shiraiwa, M.: Hydroxyl radicals from secondary organic aerosol decomposition in
740   water, Atmospheric Chemistry and Physics, 16, 1761-1771, 10.5194/acp-16-1761-2016, 2016.
741 van Pinxteren, D., Neususs, C., and Herrmann, H.: On the abundance and source contributions of
742   dicarboxylic acids in size-resolved aerosol particles at continental sites in central Europe,
743   Atmospheric Chemistry and Physics, 14, 3913-3928, 10.5194/acp-14-3913-2014, 2014.
744 Wang, G., Cheng, C., Meng, J., Huang, Y., Li, J., and Ren, Y.: Field observation on secondary organic
745   aerosols during Asian dust storm periods: Formation mechanism of oxalic acid and related
746   compounds on dust surface, Atmospheric Environment, 113, 169-176, 2015.
747 Wang, G., Zhang, R., Gomez, M. E., Yang, L., Levy Zamora, M., Hu, M., Lin, Y., Peng, J., Guo, S.,
748   Meng, J., Li, J., Cheng, C., Hu, T., Ren, Y., Wang, Y., Gao, J., Cao, J., An, Z., Zhou, W., Li, G.,
749   Wang, J., Tian, P., Marrero-Ortiz, W., Secrest, J., Du, Z., Zheng, J., Shang, D., Zeng, L., Shao, M.,
750   Wang, W., Huang, Y., Wang, Y., Zhu, Y., Li, Y., Hu, J., Pan, B., Cai, L., Cheng, Y., Ji, Y., Zhang, F.,
751   Rosenfeld, D., Liss, P. S., Duce, R. A., Kolb, C. E., and Molina, M. J.: Persistent sulfate formation
752   from London Fog to Chinese haze, Proceedings of the National Academy of Sciences, 113,
753   13630-13635, 10.1073/pnas.1616540113, 2016.
754 Wang, G. H., Kawamura, K., Cheng, C. L., Li, J. J., Cao, J. J., Zhang, R. J., Zhang, T., Liu, S. X., and
755   Zhao, Z. Z.: Molecular Distribution and Stable Carbon Isotopic Composition of Dicarboxylic
756   Acids, Ketocarboxylic Acids, and alpha-Dicarbonyls in Size-Resolved Atmospheric Particles
757   From Xi'an City, China, Environmental Science & Technology, 46, 4783-4791,
758   10.1021/es204322c, 2012.
759 Wang, J. Y., Wang, G. H., Gao, J., Wang, H., Ren, Y. Q., Li, J. J., Wu, C., Zhang, L., Wang, S. L., and
760   Chai, F. H.: Concentrations and stable carbon isotope compositions of oxalic acid and related SOA
761   in Beijing before, during and after the 2014 APEC, Atmospheric Chemistry and Physics 17,
762   981-992, 2017.
763 Weller, C., Tilgner, A., Brauer, P., and Herrmann, H.: Modeling the Impact of Iron-Carboxylate
764   Photochemistry on Radical Budget and Carboxylate Degradation in Cloud Droplets and Particles,
765   Environmental Science & Technology, 48, 5652-5659, 10.1021/es4056643, 2014.
766 Wonaschuetz, A., Sorooshian, A., Ervens, B., Chuang, P. Y., Feingold, G., Murphy, S. M., de Gouw, J.,
767   Warneke, C., and Jonsson, H. H.: Aerosol and gas re-distribution by shallow cumulus clouds: An
768   investigation using airborne measurements, Journal of Geophysical Research-Atmospheres, 117,
769   10.1029/2012jd018089, 2012.
770 Xue, J., Lau, A. K. H., and Yu, J. Z.: A study of acidity on PM2.5 in Hong Kong using online ionic
771   chemical composition measurements, Atmospheric Environment, 45, 7081-7088,
772   10.1016/j.atmosenv.2011.09.040, 2011.
773 Yang, F., Chen, H., Wang, X., Yang, X., Du, J., and Chen, J.: Single particle mass spectrometry of
774   oxalic acid in ambient aerosols in Shanghai: Mixing state and formation mechanism, Atmospheric
775   Environment, 43, 3876-3882, 2009.
776 Yao, X. H., Fang, M., and Chan, C. K.: Size distributions and formation of dicarboxylic acids in
777   atmospheric particles, Atmospheric Environment, 36, 2099-2107, 2002.
778 Yao, X. H., Lau, A. P. S., Fang, M., Chan, C. K., and Hu, M.: Size distributions and formation of ionic
779   species in atmospheric particulate pollutants in Beijing, China: 2 - dicarboxylic acids,
780   Atmospheric Environment, 37, 3001-3007, 10.1016/s1352-2310(03)00256-5, 2003.
781 Yu, J. Z., Huang, X. F., Xu, J. H., and Hu, M.: When aerosol sulfate goes up, so does oxalate:

782   Implication for the formation mechanisms of oxalate, Environmental Science & Technology, 39,

783   128-133, 10.1021/Es049559f, 2005.

784   Yu, L., Smith, J., Laskin, A., Anastasio, C., Laskin, J., and Zhang, Q.: Chemical characterization of

785   SOA formed from aqueous-phase reactions of phenols with the triplet excited state of carbonyl

786   and hydroxyl radical, Atmospheric Chemistry and Physics, 14, 13801-13816,

787   10.5194/acp-14-13801-2014, 2014.

788   Zauscher, M. D., Wang, Y., Moore, M. J. K., Gaston, C. J., and Prather, K. A.: Air Quality Impact and

789   Physicochemical Aging of Biomass Burning Aerosols during the 2007 San Diego Wildfires,

790   Environmental Science & Technology, 47, 7633-7643, 10.1021/es4004137, 2013.

791   Zhang, G., Bi, X., Li, L., Chan, L. Y., Li, M., Wang, X., Sheng, G., Fu, J., and Zhou, Z.: Mixing state of

792   individual submicron carbon-containing particles during spring and fall seasons in urban

793   Guangzhou, China: a case study, Atmospheric Chemistry and Physics, 13, 4723-4735, 2013.

794   Zhang, G., Bi, X., He, J., Chen, D., Chan, L. Y., Xie, G., Wang, X., Sheng, G., Fu, J., and Zhou, Z.:

795   Variation of secondary coatings associated with elemental carbon by single particle analysis,

796   Atmospheric Environment, 92, 162-170, 2014.

797   Zhang, R., Wang, G., Guo, S., Zamora, M. L., Ying, Q., Lin, Y., Wang, W., Hu, M., and Wang, Y.:

798   Formation of urban fine particulate matter, Chem Rev, 115, 3803-3855, 2015.

799   Zhou, Y., Huang, X. H., Bian, Q., Griffith, S. M., Louie, P. K., and Yu, J. Z.: Sources and atmospheric

800   processes impacting oxalate at a suburban coastal site in Hong Kong: Insights inferred from 1 year

801   hourly measurements, Journal of Geophysical Research: Atmospheres, 120, 9772-9788, 2015.

802

803

804

805

806

807

808

809

810

811

812

813

814

815

816

817

818

819

820

821

822

823

824

825

826 **Tables and Figures**

827

828 **Table list:**

829

830 Table 1. Summary of major groups of oxalic acid-containing particles in summer and

831 winter in PRD, China.

832

833 Table 2. The abundance of major particle types in total oxalic acid-containing

834 particles during the episode in winter (2/8/2015).

835

836 **Figure caption:**

837

838 Figure 1. Temporal variations of total detected particles and oxalic acid containing

839 particles during whole sampling periods in Heshan, China: (a) hourly variations of

840 $PM_{2.5}$ mass concentration, total detected particle counts, oxalic acid containing

841 particles, ratio of oxalic acid-containing/total particles and major types of oxalic acid

842 containing particles; (b) variation patterns of relative abundance of major types of

843 oxalic acid containing particles.

844

845 Figure 2. The averaged positive and negative ion mass spectra of oxalic acid

846 containing particles is investigated in summer and winter: (a) summer positive, (b)

847 summer negative, (c) winter positive, (d) winter negative. The color bars represent

848 each peak area corresponding to specific fraction in individual particles.

849

850 Figure 3. (a) Mixing state of oxalic acid with sulfate, nitrate and ammonium in oxalic

851 acid-containing particles; (b) Linear correlation between NH_4^+-containing oxalic acid

852 particles and the total oxalic acid particles in summer; (c) Linear correlation between

853 NH_4^+-containing oxalic acid particles and the total oxalic acid particles in winter.

854 Abbreviations: C_2-NH_4^+ represents the NH_4^+-containing oxalic acid particles, and

855 same expressions for C_2-SO_4^{2-} and C_2-NO_3^-.

856

Figure 4. Unscaled size-resolved number distributions of major types of oxalic acid particles in summer and winter.

Figure 5. Temporal variations of O_3 concentrations, oxalic acid particles, malonic acid particles and heavy metal type of oxalic acid particles during the entire sampling period in Heshan, China.

Figure 6. The averaged digitized positive and negative ion mass spectra of heavy metal type of oxalic acid-containing particles in summer.

Figure 7. The diurnal variations of O_3 concentration, oxalic acid particles, HM group particles and in-situ pH (pH_{is}) from July 28 to August 1 in 2014.

Figure 8. The diurnal variations of peak area of iron (m/z=56) and oxalic acid (m/z=-89) in the HM type oxalic acid particles from July 28 to August 1, 2014.

Figure 9. The temporal variations of peak area of nitrate, sulfate and oxalic acid, and the relative acidity ratio (R_{ra}) in carbonaceous type oxalic acid particles in winter.

Figure 10. The comprehensive study of oxalic acid particles increase on Feb 8, 2015: (a) The digitized positive and negative ion mass spectrum of oxalic acid particles during the episode; (b) Linear regression between total oxalic acid particles and organosulfate-containing oxalic acid particles (m/z -155).

887

888

889

890

Table 1. Summary of major groups of oxalic acid-containing particles in summer and winter in PRD, China.

Particle type	Summer(7/18-8/1, 2014)		Winter(1/27-2/8, 2015)	
	Count	Percentage, %	Count	Percentage, %
EC	1473	11.2	3161	15.4
ECOC	41	0.3	2233	10.9
OC	473	3.6	1922	9.4
BB	1702	13.0	4953	24.2
HM	4104	31.3	3124	15.2
Sec	2511	19.2	2192	10.7
NaK	303	2.3	17	0.1
Dust	1139	8.7	1888	9.2

Abbreviations of major particle types: elemental carbon (EC), elemental and organic carbon (ECOC), organic carbon (OC), biomass burning (BB), heavy metal (HM), secondary (Sec), sodium and potassium (NaK) and dust (Dust).

891

892

893

894

895

Table 2. The abundance of major particle types in total oxalic acid-containing particles during the episode in winter (2/8/2015).

	EC	ECOC	OC	BB	Sec	HM	Dust	other
Count	1250	604	326	1320	856	377	814	132
Percentage, %	22.0	10.6	5.7	23.2	15.1	6.6	14.3	2.3

896

897

898

899

900

901

902

903

904

905

906

907

908
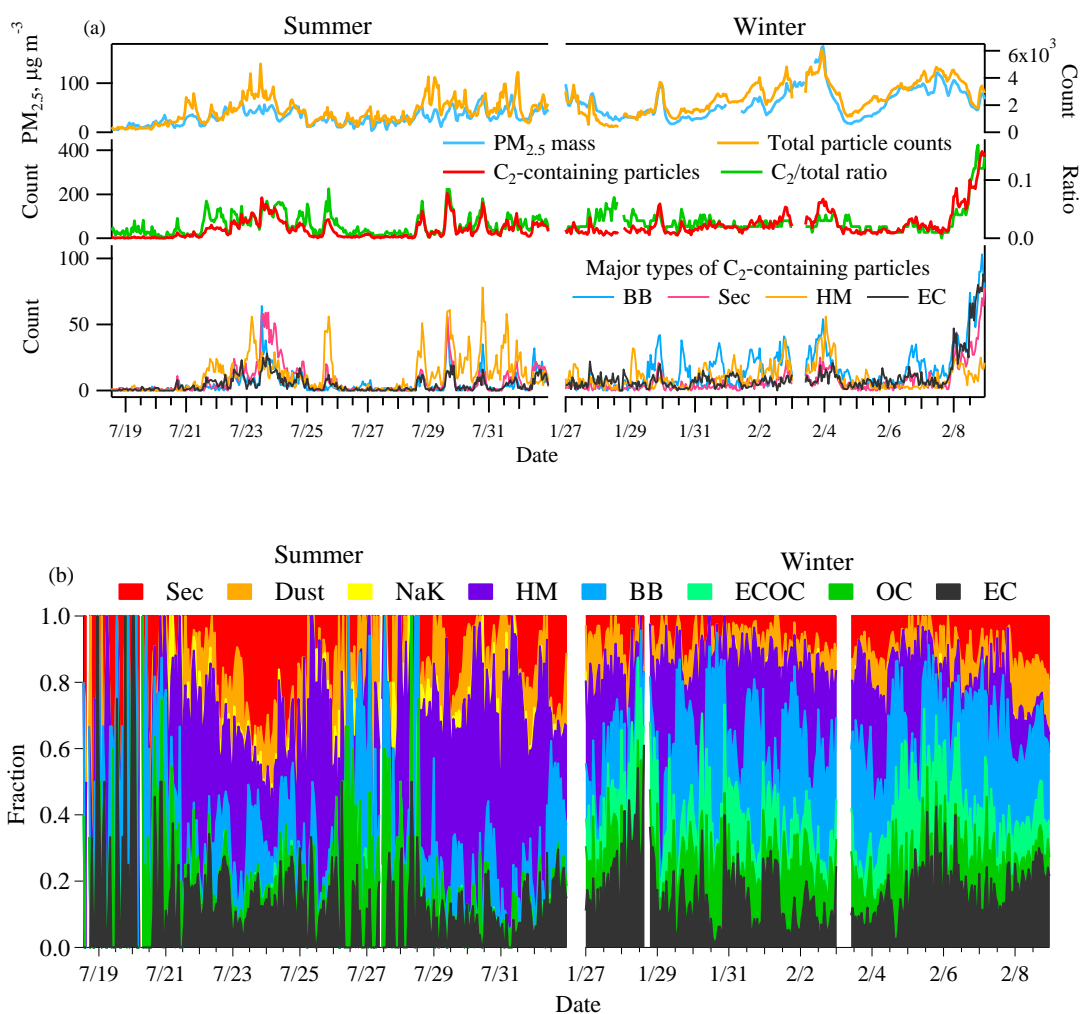
909
910

911

Figure 1. Temporal variations of total detected particles and oxalic acid containing particles during whole sampling periods in Heshan, China: (a) hourly variations of PM$_{2.5}$ mass concentration, total detected particle counts, oxalic acid containing particles, ratio of oxalic acid-containing/total particles and major types of oxalic acid containing particles; (b) variation patterns of relative abundance of major types of oxalic acid containing particles. Abbreviations of major particle types: elemental carbon (EC), organic carbon (OC), elemental and organic carbon (ECOC), biomass burning (BB), heavy metal (HM), secondary (Sec), sodium and potassium (NaK) and dust.

921
922
923
924
925

Figure 2. The averaged positive and negative ion mass spectra of oxalic acid containing particles is investigated in summer and winter: (a) summer positive, (b) summer negative, (c) winter positive, (d) winter negative. The color bars represent each peak area corresponding to specific fraction in individual particles.

956
957

958

Figure 3. (a) Mixing state of oxalic acid with sulfate, nitrate and ammonium in oxalic acid-containing particles; (b) Linear correlation between NH_4^+-containing oxalic acid particles and the total oxalic acid particles in summer; (c) Linear correlation between NH_4^+-containing oxalic acid particles and the total oxalic acid particles in winter. Abbreviations: C_2-NH_4^+ represents the NH_4^+-containing oxalic acid particles, and same expressions for C_2-SO_4^{2-} and C_2-NO_3^-.

965

966

967

968

969

970

971

972

973

974

975

976

977

978

979
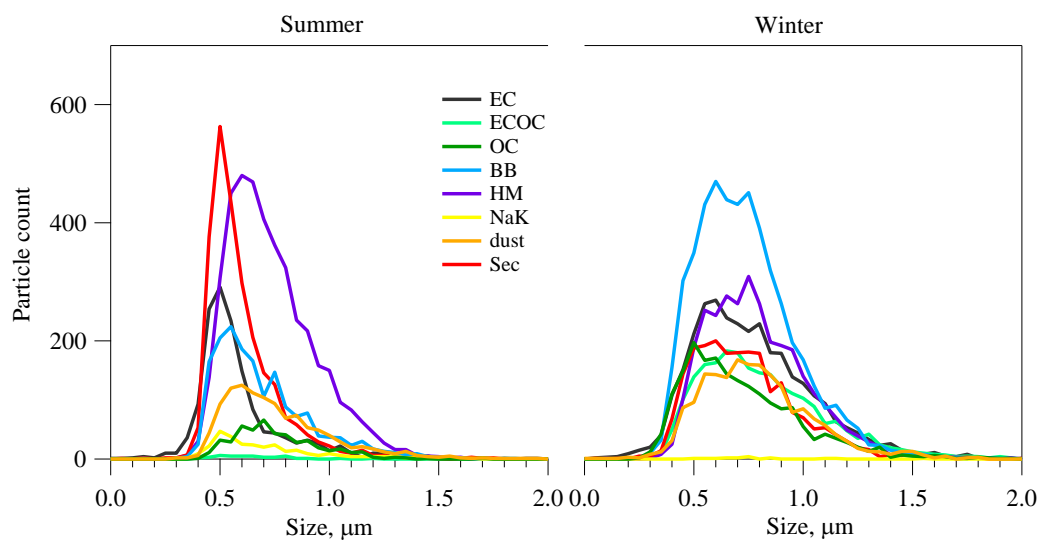
980

Figure 4. Unscaled size-resolved number distributions of major types of oxalic acid particles in summer and winter. Abbreviations of major particle types: elemental carbon (EC), organic carbon (OC), elemental and organic carbon (ECOC), biomass burning (BB), heavy metal (HM), secondary (Sec), sodium and potassium (NaK) and dust.

986
987
988
989
990
991
992
993
994
995
996
997
998
999
1000
1001
1002
1003
1004

1007
1008
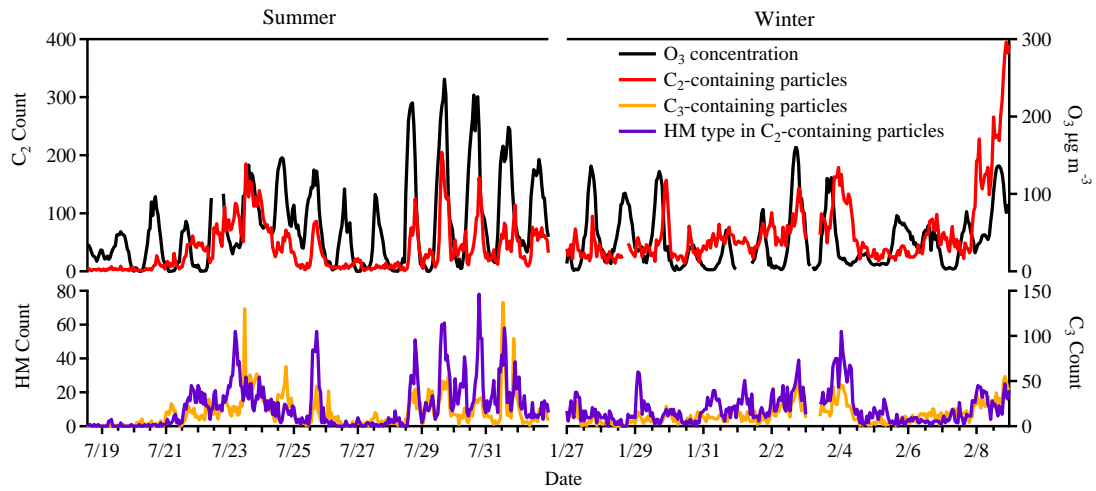
1009   Figure 5. Temporal variations of O_3 concentrations, oxalic acid particles, malonic acid

1010   particles and heavy metal type of oxalic acid particles during the entire sampling

1011   period in Heshan, China.

1012
1013
1014
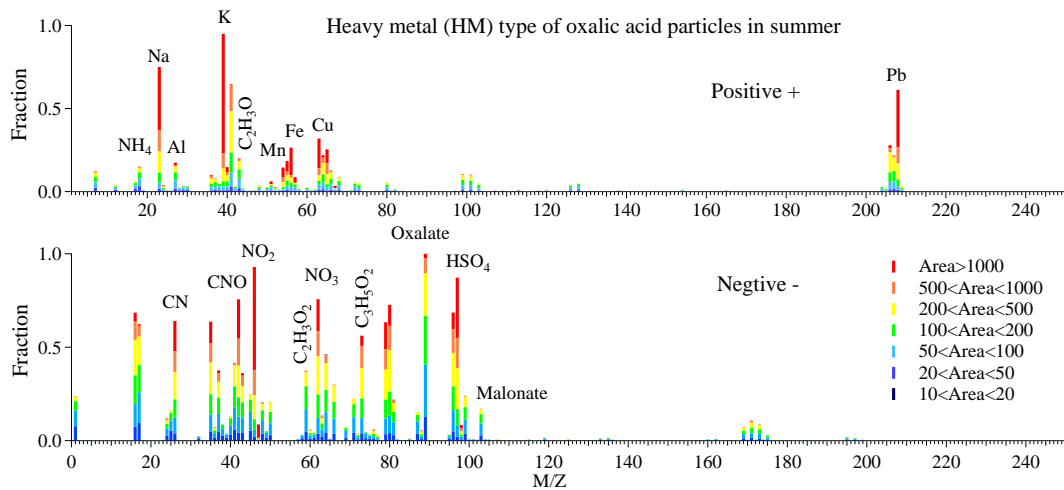
1015

1016   Figure 6. The averaged digitized positive and negative ion mass spectra of heavy

1017   metal type of oxalic acid-containing particles in summer.

1018
1019
1020
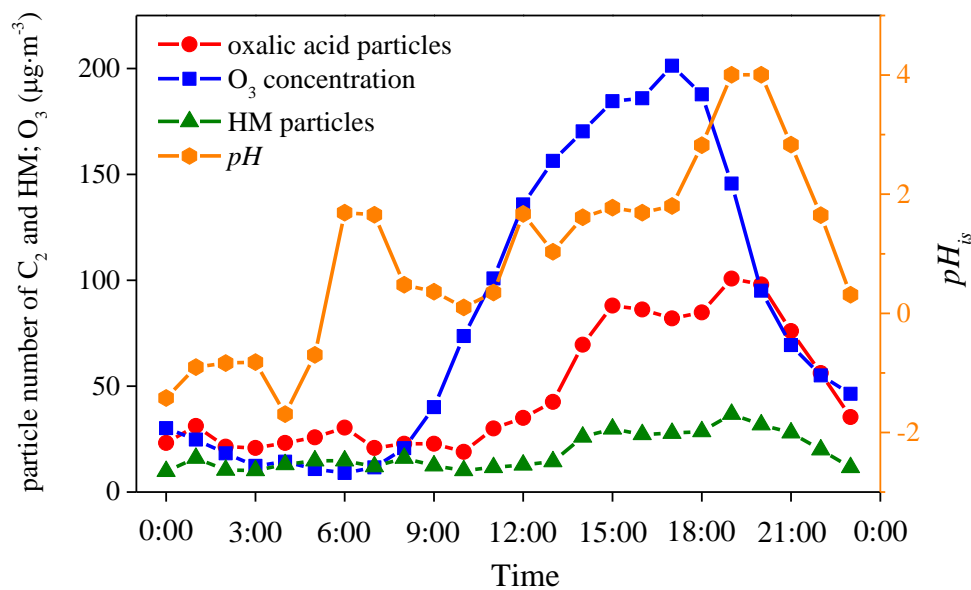
1021

1022 Figure 7. The diurnal variations of O₃ concentration, oxalic acid particles, HM group

1023 particles and in-situ pH (pH_{is}) from July 28 to August 1 in 2014.

1024

1025

1026

1027

1028
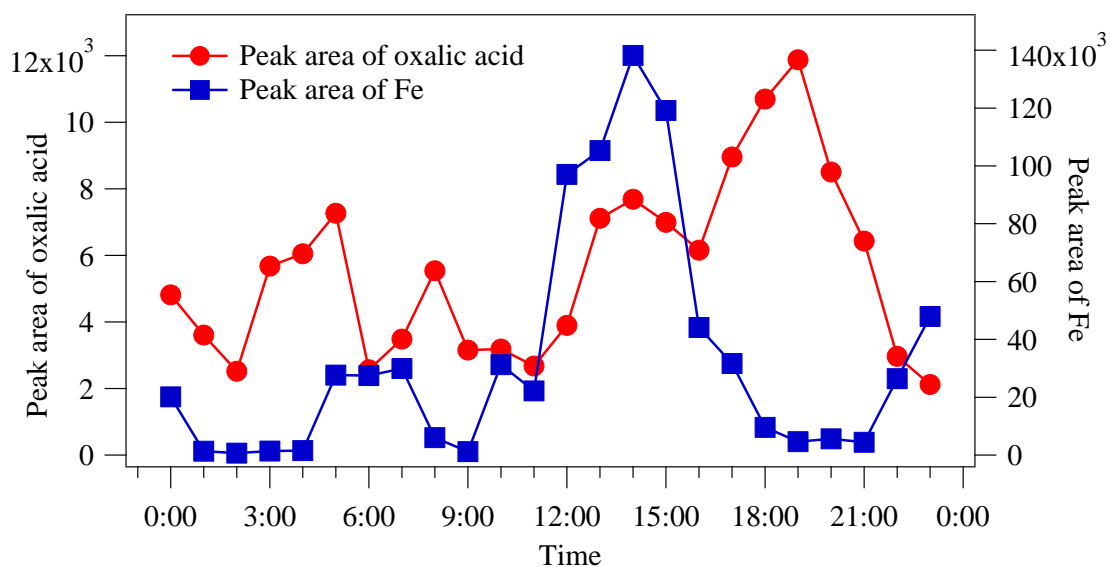
1029

1030 Figure 8. The diurnal variations of peak area of iron (m/z=56) and oxalic acid

1031 (m/z=-89) in the HM type oxalic acid particles from July 28 to August 1, 2014.

1032

1033
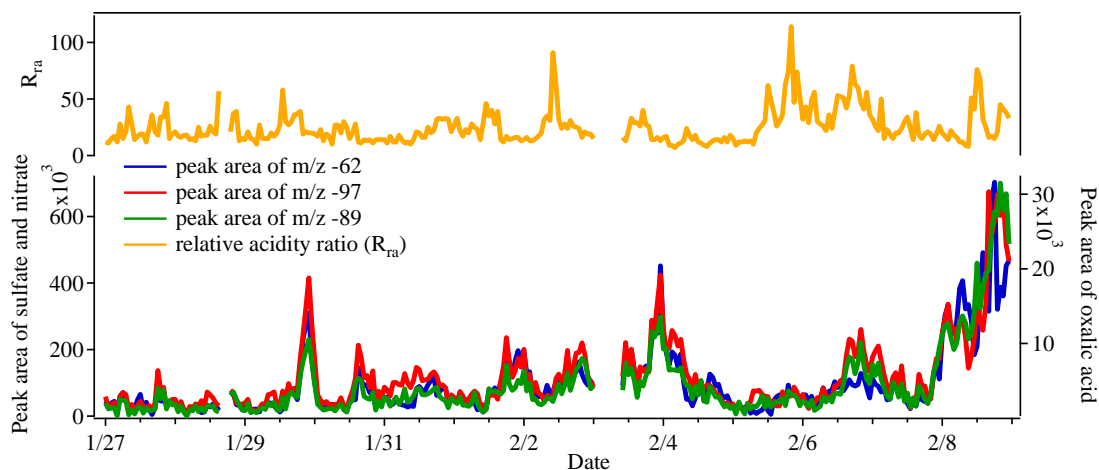
1034

1035 Figure 9. The temporal variations of peak area of nitrate, sulfate and oxalic acid, and

1036 the relative acidity ratio (R_{ra}) in carbonaceous type oxalic acid particles in winter.

1037
1038
1039
1040
1041
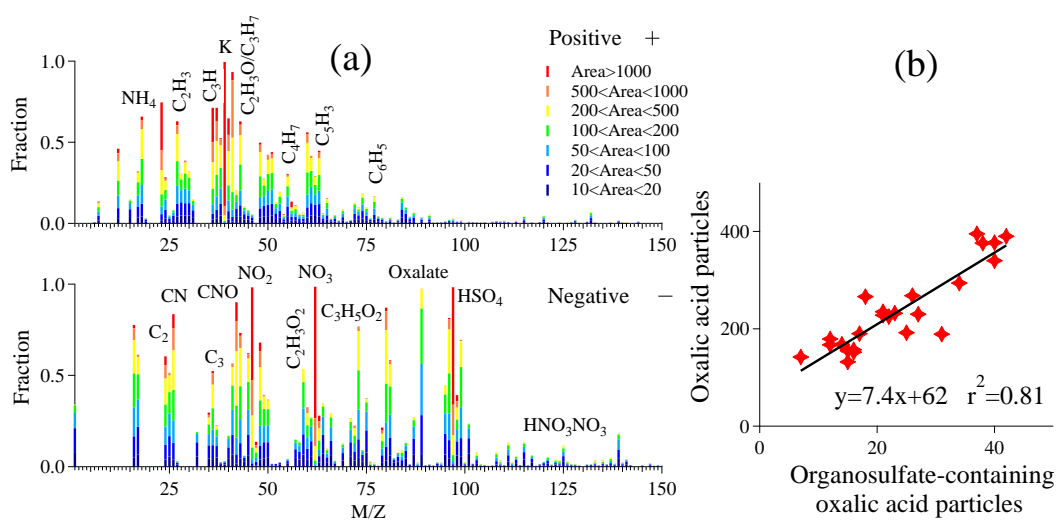
1042

1043 Figure 10. The comprehensive study of oxalic acid particles increase on Feb 8, 2015:

1044 (a) The digitized positive and negative ion mass spectrum of oxalic acid particles

1045 during the episode; (b) Linear regression between total oxalic acid particles and

1046 organosulfate-containing oxalic acid particles (m/z -155).

1047
1048